Palladium Nanoparticle Formation on TiO$_2$(110) by Thermal Decomposition of Palladium(II) Hexafluoroacetylacetonate

Amir Gharachorlou,[†] Michael D. Detwiler,[†] Anna V. Nartova,[†,‡,§] Yu Lei,[⊥] Junling Lu,[⊥] Jeffrey W. Elam,[⊥] W. Nicholas Delgass,[†] Fabio H. Ribeiro,[†] and Dmitry Y. Zemlyanov*,[∥]

[†]School of Chemical Engineering, Purdue University, West Lafayette, Indiana 47907, United States
[‡]Boreskov Institute of Catalysis, Novosibirsk 630090, Russia
[§]Novosibirsk State University, Novosibirsk 630090, Russia
[⊥]Energy Systems Division, Argonne National Laboratory, Argonne, Illinois 60439, United States
[∥]Birck Nanotechnology Center, Purdue University, West Lafayette, Indiana 47907, United States

Ⓢ Supporting Information

ABSTRACT: Palladium nanoparticles were synthesized by thermal decomposition of palladium(II) hexafluoroacetylacetonate (Pd(hfac)$_2$), an atomic layer deposition (ALD) precursor, on a TiO$_2$(110) surface. According to X-ray photoelectron spectroscopy (XPS), Pd(hfac)$_2$ adsorbs on TiO$_2$(110) dissociatively yielding Pd(hfac)$_{ads}$, hfac$_{ads}$, and adsorbed fragments of the hfac ligand at 300 K. A (2 × 1) surface overlayer was observed by scanning tunneling microscopy (STM), indicating that hfac adsorbs in a bidentate bridging fashion across two Ti 5-fold atoms and Pd(hfac) adsorbs between two bridging oxygen atoms on the surface. Annealing of the Pd(hfac)$_{ads}$ and hfac$_{ads}$ species at 525 K decomposed the adsorbed hfac ligands, leaving PdO-like species and/or Pd atoms or clusters. Above 575 K, the XPS Pd 3d peaks shift toward lower binding energies and Pd nanoparticles are observed by STM. These observations point to the sintering of Pd atoms and clusters to Pd nanoparticles. The average height of the Pd nanoparticles was 1.2 ± 0.6 nm at 575 K and increased to 1.7 ± 0.5 nm following annealing at 875 K. The Pd coverage was estimated from XPS and STM data to be 0.05 and 0.03 monolayers (ML), respectively, after the first adsorption/decomposition cycle. The amount of palladium deposited on the TiO$_2$(110) surface increased linearly with the number of adsorption/decomposition cycles with a growth rate of 0.05 ML or 0.6 Å per cycle. We suggest that the removal of the hfac ligand and fragments eliminates the nucleation inhibition of Pd nanoparticles previously observed for the Pd(hfac)$_2$ precursor on TiO$_2$.

KEYWORDS: X-ray photoelectron spectroscopy, scanning tunneling microscopy, atomic layer deposition, Pd(hfac)$_2$, TiO$_2$(110), nucleation delay, surface science, heterogeneous catalysis
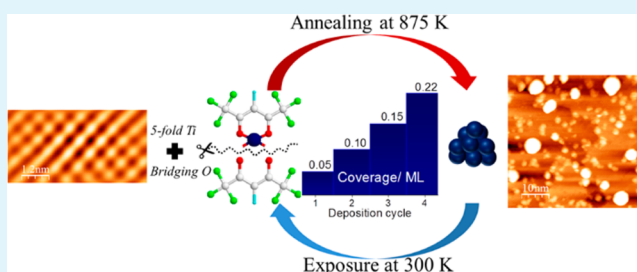
1. INTRODUCTION

Palladium is used for numerous catalytic applications including carbon−carbon coupling,[1] hydrocarbon hydrogenation and dehydrogenation,[2,3] hydrocarbon oxidation and combustion,[4,5] and the purification of automotive exhaust gases.[6] Recently, atomic layer deposition (ALD) has emerged as a technique promising greater control for synthesis of nanometer and subnanometer transition metal particles including Pd on oxide supports for heterogeneous catalysis.[7−13] Primarily used to grow thin films, ALD is based on self-limiting surface reactions in which a surface is alternately exposed to different precursors separated by purging inert gas or vacuum, providing atomically controlled growth.[14] Nanoparticles can be grown on oxide supports during early stages of ALD processes for heterogeneous catalysis applications. Palladium nanoparticles synthesized by ALD using palladium(II) hexafluoroacetylacetonate (Pd(hfac)$_2$) as a Pd precursor demonstrated higher selectivity toward desired products and particle stability compared to

traditionally prepared catalysts in reactions such as methanol decomposition,[10] ethanol and isopropyl alcohol oxidation,[13] and oxidative dehydrogenation of alkanes.[9]

Formation of nanoparticles from (hfac)-based organometallic precursors has exhibited a nucleation delay and requires a high number of ALD cycles (∼100 cycles) that limits its large scale application. Different characterization techniques have been used to isolate the surface intermediates and identify the surface active sites during the initial precursor exposure. Fourier transform infrared (FTIR) measurements suggested that Pd(hfac)$_2$ decomposes to Pd(hfac)$_{ads}$ and Al(hfac)$_{ads}$ upon adsorption on Al$_2$O$_3$ and the resulting nucleation delay period was assigned to possible surface poisoning with Al(hfac)$_{ads}$ species.[8,15,16] Using gas-phase infrared spectroscopy, Weber et

al. suggested that H_2+O_2 plasma is required to remove the hfac ligands and other carbon moieties left from $Pd(hfac)_2$ adsorption on Al_2O_3.[17] Adsorbed hfac ligands were also suggested to block adsorption sites on TiO_2 for Pt particle formation using $Pt(hfac)_2$ as the precursor.[18]

In addition to surface intermediates, the substrate chemistry can also change the growth behavior of the (hfac)-based precursors. Pd nucleation is faster on ZnO than Al_2O_3 at the same conditions. 100 ALD Pd cycles on ZnO yields Pd islands with 10 to 20 nm domains. However, 200 cycles were required to form islands consisting of 10 nm domains on Al_2O_3.[10] X-ray photoelectron spectroscopy (XPS) studies of $Cu(hfac)_2$ adsorption on Pt(111) showed chemical differences compared to the $Cu(hfac)_2$ on copper and TiO_2 systems. The hfac group formed on copper and TiO_2 surfaces remained intact until 373 and 473 K, respectively, whereas hfac species formed on Pt(111) showed significant decomposition by 300 K.[19,20] Moreover, surface contamination existing prior to deposition has been shown to influence the decomposition pathway and the final structure of nanoparticles. X-ray absorption spectroscopy (XAS) showed, for example, that residual chlorine on the TiO_2 surface can participate in the decomposition pathway of $Pd(hfac)_2$. In the presence of chlorine, $Pd(hfac)_2$ decomposed to form $Pd(hfac)Cl_{2ads}$ and $Ti(hfac)_{ads}$ species.[21]

All of these studies demonstrate that the initial substrate−$Pd(hfac)_2$ interaction and existing surface species play a major role in tailoring the final properties of the nanoparticles and the Pd growth behavior. As recently highlighted by Zaera,[22] fundamental surface science studies can serve as an ideal tool to understand the intermediates involved in the deposition mechanism, and for elucidating how the overall precursor-substrate interaction process takes place during the initial exposure of the precursor.

In this work, Pd(II) hexafluoroacetylacetonate ($Pd(hfac)_2$) was used for synthesis of Pd nanoparticles on the $TiO_2(110)$ surface. The evolution of the organometallic precursor was monitored by surface sensitive characterization techniques including X-ray photoelectron spectroscopy (XPS) and scanning tunneling microscopy (STM) to better understand the adsorption and thermal decomposition pathways of $Pd(hfac)_2$ on $TiO_2(110)$ surface, as well as to track the formation of Pd nanoparticles (NPs).

2. EXPERIMENTAL METHODS

2.1. Instruments. Experiments were performed in two separate UHV systems. An Omicron Surface Analysis Cluster at Birck Nanotechnology Center (BNC), Purdue University, consisting of an ultrahigh vacuum (UHV) preparation chamber and μ-metal analysis chamber with base pressures of 1×10^{-9} and 5×10^{-11} mbar, respectively, was used for XPS analysis. The preparation chamber was equipped with a mass spectrometer, an Ar^+ sputtering gun, resistive sample heating, and a leak valve for dosing ALD precursors. The analysis chamber was equipped with XPS, low energy electron diffraction (LEED), high resolution electron energy loss spectroscopy (HREELS), and resistive sample heating. The second experimental apparatus at the Center for Nanoscale Materials (CNM), Argonne National Laboratory, was an Omicron VT SPM system equipped with a variable temperature STM/AFM (Omicron VT-SPM XA), a preparation chamber for dosing ALD precursors through a leak valve, an Ar^+ sputtering gun, and resistive sample heating. The base pressure in the STM and preparation chambers was $\leq 5 \times 10^{-11}$ mbar. STM images were obtained using etched W tips. STM images were analyzed using WSxM software.[23] Pymol software (version 1.5.0.4) was used for molecular visualization.

$TiO_2(110)$ single crystals of 9 mm diameter and 1 mm thickness (Princeton Scientific Corp.) were used. In both systems, the sample cleaning procedure consisted of repeated cycles of Ar^+ sputtering and vacuum annealing at 925 K. For the XPS study, sample temperature was measured by a K-type thermocouple spot-welded to the stainless steel backplate, and crystal cleanliness was monitored by XPS and LEED. The appearance of the fresh crystal changed from transparent to light blue following several cleaning cycles, the signature of a slightly reduced crystal.[24]

$TiO_2(110)$ crystals were exposed to Pd(II) hexafluoroacetylaceto-nate ($Pd(hfac)_2$) (Aldrich, 99.9%) in the preparation chambers of both systems. $Pd(hfac)_2$ powder was loaded into a miniature 50 mL Swagelok stainless steel cylinder and was pumped by a turbo pump several times before each dosing. All gas lines were regularly heated overnight at 423 K. For the XPS experiment, dosing was performed through a leak valve for 10 min at a pressure of $\sim 5 \times 10^{-7}$ mbar for an exposure of 225 L to ensure saturation. Higher exposures of $Pd(hfac)_2$ did not change surface Pd coverage. Dosing pressure was determined during a test experiment, and the ion gauge was kept off during $Pd(hfac)_2$ exposure to avoid electron-induced decomposition of $Pd(hfac)_2$. For the STM experiment, the maximum achievable $Pd(hfac)_2$ base pressure was much lower ($\sim 4 \times 10^{-9}$ mbar) due to system geometry differences; however, the sample sat ~ 2 in. away from a dosing capillary aimed at the sample. $Pd(hfac)_2$ was dosed at approximately this pressure for 60 min to ensure saturation.

XPS data were acquired using a nonmonochromatic Mg Kα X-ray source ($h\nu$ = 1253.6 eV) at 150 W. High resolution spectra were recorded at a constant pass energy of 20 eV. The resolution, defined as the full-width at half-maximum (fwhm) of the Ti $2p_{3/2}$ peak, was approximately 1.1 eV. Unfortunately, no energy scale correction was foreseen by the analyzer manufacturer (analyzer, Omicron EAC 125; controller, Omicron EAC 2000), and therefore it was possible only to set the Au $4f_{7/2}$ peak at 84.0 eV by changing the spectrometer work function. Slight sample charging was corrected by fixing the Ti $2p_{3/2}$ peak at 459.3 eV.

XPS data were analyzed with CasaXPS (version 2313Dev64) software. Curve fitting was done assuming a Gaussian/Lorentzian line shape (30% Lorentzian, CasaXPS function: SGL(30)) for symmetric peaks and an asymmetric Lorentzian shape (CasaXPS function: LF(1,1.5,25,70)) for asymmetric peaks.

2.2. Coverage Calculations. Because an adlayer on a surface is represented as an adsorbed layer on a semi-infinite substrate, traditional XPS quantification, which assumes homogeneous elemental distribution within the information depth, is not appropriate. To quantify the XPS result, we followed Fadley's approach,[25] which assumes a nonattenuating adlayer at fractional coverage. Coverage (Θ), measured in monolayers (ML), is the ratio between the number of adsorbed species and the number of surface atoms, and can be expressed as

$$\Theta = \frac{N_l(\theta) \times \Omega_s(E_s) \times A_S(E_s) \times \frac{d\sigma_s}{d\Omega} \times \Lambda_e^{subst}(E_s) \times \cos\theta}{N_s(\theta) \times \Omega_l(E_l) \times A_l(E_l) \times \frac{d\sigma_l}{d\Omega} \times d_s}$$

(1)

where $N_l(\theta)$ and $N_s(\theta)$ are the photoemission peak areas of the adlayer and the substrate at the given photoemission angle, θ, with respect to the surface normal; $d\sigma_l/d\Omega$ and $d\sigma_s/d\Omega$ are differential cross sections for the photoemission peaks of the adlayer and the substrate, which can be calculated using tabulated Scofield cross sections[26] and Reilman asymmetry parameters;[27] $\Lambda_e^{subst}(E_s)$ is the electron attenuation length (EAL) of the photoelectrons originating from the substrate atom that have traveled through the substrate material, and d_s is the interlayer distance of the substrate. The EAL was calculated by NIST SRD-82.[28] The required parameters and the derivation of eq 1 can be found in Table S1 and XPS coverage and thickness model derivations provided in the Supporting Information.
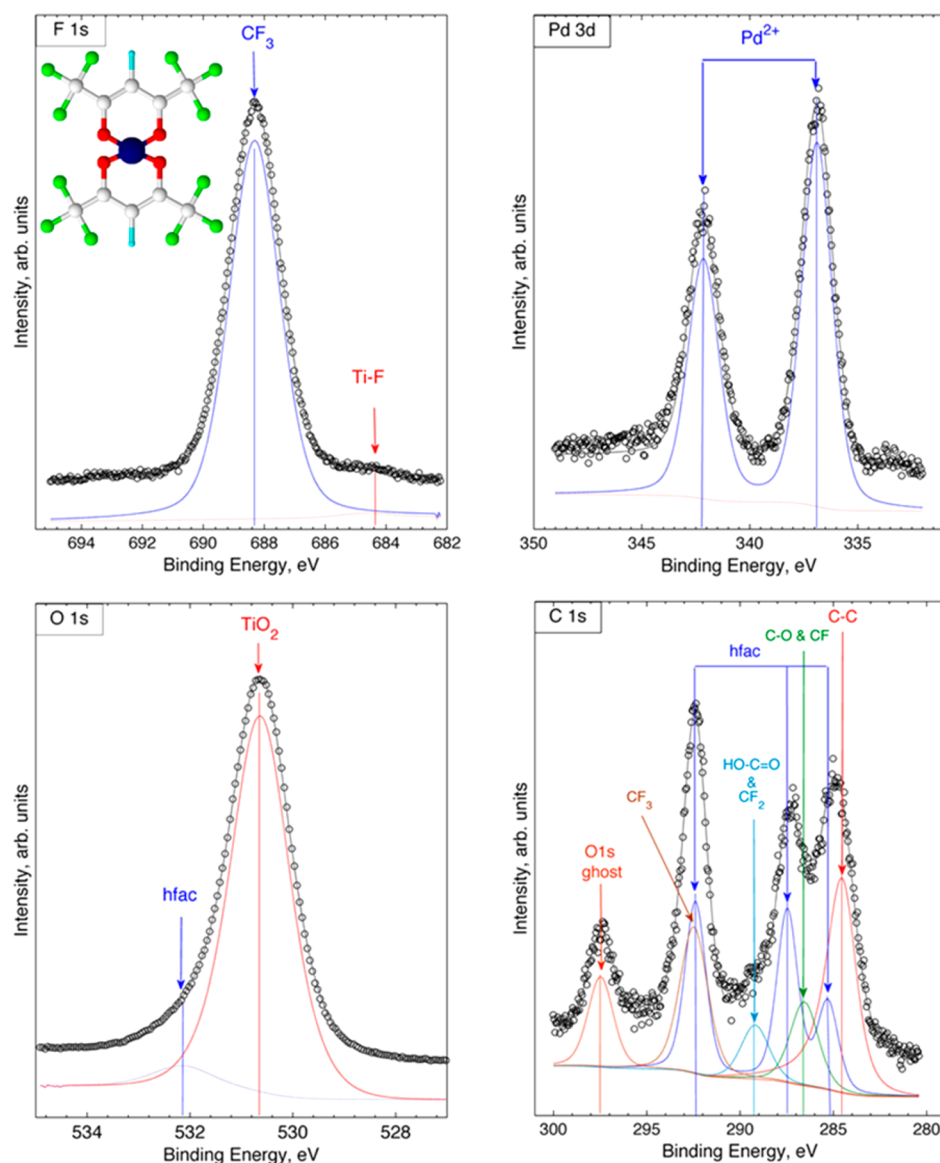
Figure 1. F 1s, O 1s, Pd 3d, and C 1s photoemission spectra obtained after exposure of the $TiO_2(110)$ surface to $Pd(hfac)_2$ up to saturation at 300 K. Ball and stick schematic of $Pd(hfac)_2$ molecule is shown inside F 1s region (Pd atom, blue; O atoms, red; C atoms, white; F atoms, lime; H atoms, cyan).

Table 1. Characteristic XPS Features Observed after $Pd(hfac)_2$ Adsorption at Room Temperature and Its Subsequent Thermal Decomposition

species	binding energy, eV				
	C 1s	F 1s	Pd $3d_{5/2}$	O 1s	Ti $2p_{3/2}$
$Pd(hfac)_{ads}$	285.2 (C−H)	688.3	336.9	532.1	
	287.5 (C=O)				
	292.4 (CF_3)				
TiO_2				530.6	459.3
cracked fragments of $Pd(hfac)_2$					
CF_3	292.5	688.3			
CF_2, HO−C=O	289.2				
CF, CO	286.4				
C−H, C−C	284.5				
TiF_x		684.9			
PdO_x and Pd NPs			336.2−335.5		
artifact					
O 1s ghost peak from Al $K\alpha$	ca. 297.5				

3. RESULTS

3.1. X-ray Photoelectron Spectroscopy. Figure 1 shows XPS spectra of the F 1s, O 1s, Pd 3d, and C 1s core-levels obtained after saturation exposure of the $TiO_2(110)$ surface to $Pd(hfac)_2$ at 300 K. The structure of the $Pd(hfac)_2$ molecule is shown inside the F 1s region in Figure 1. The main component of the F 1s peak is at 688.3 eV and represents a CF_3 functional group in hfac ligand. The minor F 1s peak detected at 684.9 eV is assigned to Ti−F.[29] The O 1s spectrum was fitted with two components at 530.6 and 532.1 eV. The former peak is a feature of TiO_2, and the latter represents oxygen atoms in the hfac ligand. Supporting this assignment, heating the sample to 575 K causes hfac ligands to decompose (discussed below), and the peak at 532.1 eV is absent. This same peak was observed following adsorption of $Cu(hfac)_2$ on the TiO_2 surface.[20] Palladium is represented by a single broad Pd $3d_{5/2}$ peak (fwhm = 1.6 eV) at 336.9 eV. The observed binding energy (BE) is slightly higher than 336.6 eV, which is the reference value for PdO (see, for instance, reference 30 and references therein). Intact $Pd(hfac)_2$ adsorbed in multilayers on a copper substrate is characterized by a Pd $3d_{5/2}$ peak at 339.1 eV;[31] therefore, the component at 336.9 eV was assigned to a palladium atom in a $Pd(hfac)_{ads}$ species. This assignment is further confirmed by XPS quantification and STM images (discussed later).

Analysis of the C 1s region revealed contributions from several species (Figure 1). The first is an hfac species, which is characterized by three components, each representing a distinct chemical state of the carbon atoms in hfac (see Figure 1). These components at 285.2, 287.5, and 292.4 eV were assigned to carbon atoms in C—H, C═O, and CF_3, respectively. Our assignments are based on Hantsche,[32] and these values are in good agreement with those observed for $Cu(hfac)_2$ and $Pd(hfac)_2$.[31,33−36] Characteristic BEs are summarized in Table 1.

To identify fragments from hfac cracking, the area ratio between the CF_3, C═O, and C—H components was constrained to 2:2:1 during curve fitting based on the stoichiometry of the hfac group (Figure 1). As shown in Figure 1, the hfac components alone were not enough for a proper fitting of the C 1s region; therefore, other components were added. The highest BE peak at approximately 297.5 eV was an O 1s ghost peak excited by Al Kα radiation (a dual Mg/Al X-ray gun was used). Inclusion of the O 1s ghost peak in the curve fitting was crucial to ensure correct background subtraction and spectrum deconvolution. The ratio between the O 1s and ghost peak areas was always constant, confirming this assignment. The O 1s ghost peak area was excluded from carbon quantification. The four other components represent decomposition fragments of the hfac group: residual carbon (carbon bonded to carbon and/or hydrogen only) is assigned to the peak at 284.5 eV, the component at 286.4 eV is a feature corresponding to C—F and/or C—O species (carbon bonded to oxygen or fluorine), CF_2 and carboxyl groups are characterized by the peak at 289.2 eV, and the peak at 292.5 eV is due to CF_3 species. Partial dissociation of the hfac species likely occurs during adsorption. Caution was taken to avoid radiation damage by minimizing exposure to the X-ray flux. Characteristic $Pd(hfac)_2$ core levels (F 1s, C 1s, Pd 3d) were collected first followed by Ti 2p and O 1s. Radiation-induced decomposition of the precursor was only observed during prolonged exposure to X-rays by the appearance of the F 1s

peak at 684.9 eV, which was a signature of precursor decomposition.

The coverage of adsorbed species was calculated using eq 1. The F 1s, Pd 3d, and C 1s peaks represented the adlayer, and the Ti 2p peaks represented the substrate. At room temperature (Figure 1), the adlayer was assumed to consist of $Pd(hfac)_{ads}$ and $hfac_{ads}$ species along with fragments of the hfac ligand. To calculate the coverage of $Pd(hfac)_{ads}$ + $hfac_{ads}$, corresponding contributions of these characteristic components were taken from the F 1s, C 1s, and O 1s peaks (hfac components only), which were obtained using the curve fittings shown in Figure 1. For Pd, the entire Pd 3d region was used for coverage calculations. The coverages of $Pd(hfac)_{ads}$ + $hfac_{ads}$ based on the F 1s, Pd 3d, and C 1s regions were equal to 0.10, 0.10, and 0.08 ML at 300 K, respectively (Table 2). The coverages were

Table 2. Coverage of hfac Species as a Function of Adsorption Temperature[a]

adsorption temperature, K	coverage, ML, calculated based on		
	Pd 3d	C 1s (the hfac component only)	F 1s (the hfac component only)
300	0.10	0.08	0.10
375	0.11	0.09	0.08
450	0.12	0.09	0.10

[a]The standard deviation of the coverage values was less than 0.004 ML. Standard deviations were calculated using standard procedures in the CasaXPS software.

normalized to the stoichiometric ratio of Pd:C:F in the $Pd(hfac)_2$ molecule (1:10:12). The other quantification parameters, for instance, the ratio between the CF_3 carbon component of C 1s and the CF_3 fluorine component of F 1s, matched the stoichiometry as well. The equal value between the normalized coverages (∼0.1 ML) for the Pd, C, and F showed that the surface species kept the original stoichiometry of the molecule and can consist of $Pd(hfac)_2$ or $Pd(hfac)_{ads}$ + $hfac_{ads}$. However, the Pd $3d_{5/2}$ XPS peak at 336.9 eV eliminates the presence of the $Pd(hfac)_2$ molecule and allows us to conclude that following $Pd(hfac)_2$ exposure at 300 K, the $TiO_2(110)$ surface is covered by the $Pd(hfac)_{ads}$ + $hfac_{ads}$ species at a coverage of approximately 0.1 ML. Cracked fragments of hfac such as C—H, C—C, C—F, C—O, CF_2, carboxyl groups, and CF_3 species were also present on the surface.

The effect of temperature on $Pd(hfac)_2$ adsorption was investigated by exposing the $TiO_2(110)$ surface to $Pd(hfac)_2$ at 300, 375, and 450 K. For higher adsorption temperatures, the extent of fragmentation of the $hfac_{ads}$ and $Pd(hfac)_{ads}$ species increased. At 300 K, the symmetric F 1s peak at 688.3 eV represents the CF_3 functional group in the hfac ligand. With increasing adsorption temperature, a peak at 684.9 eV grows, which is the signature of the Ti−F bond (spectra for different adsorption temperatures are provided in the Supporting Information, Figure S1).[29] The maximum concentration of Ti−F occurred at 450 K due to the thermal decomposition of the hfac ligand. At 300 K, a single chemical state of palladium as $Pd(hfac)_{ads}$ was observed at 336.8 eV, but a new Pd $3d_{5/2}$ peak at 336.2 eV appeared following adsorption at 375 and 450 K (Figure S1, Supporting Information). The appearance of this peak could be due to $Pd(hfac)_{ads}$ decomposition and the appearance of a PdO_x ($x < 1$) species and/or Pd clusters. The coverage of the hfac-containing species was calculated using eq

Table 3. Coverage for the Different C-Containing Species as a Function of Adsorption Temperature[a]

adsorption temperature, K	coverage, ML				
	C—F+C—O	residual HC	CF$_2$+−HO—C≡O	CF$_3$	hfac
300	0.28 ± 0.04	0.54 ± 0.03	0.16 ± 0.01	0.37 ± 0.04	0.09 ± 0.003
375	0.23 ± 0.03	0.65 ± 0.03	0.15 ± 0.02	0.39 ± 0.03	0.09 ± 0.003
450	0.33 ± 0.04	0.78 ± 0.03	0.16 ± 0.01	0.38 ± 0.04	0.09 ± 0.003

[a]The error is one standard deviation of the coverage. Standard deviations were calculated using standard procedures in the CasaXPS software.
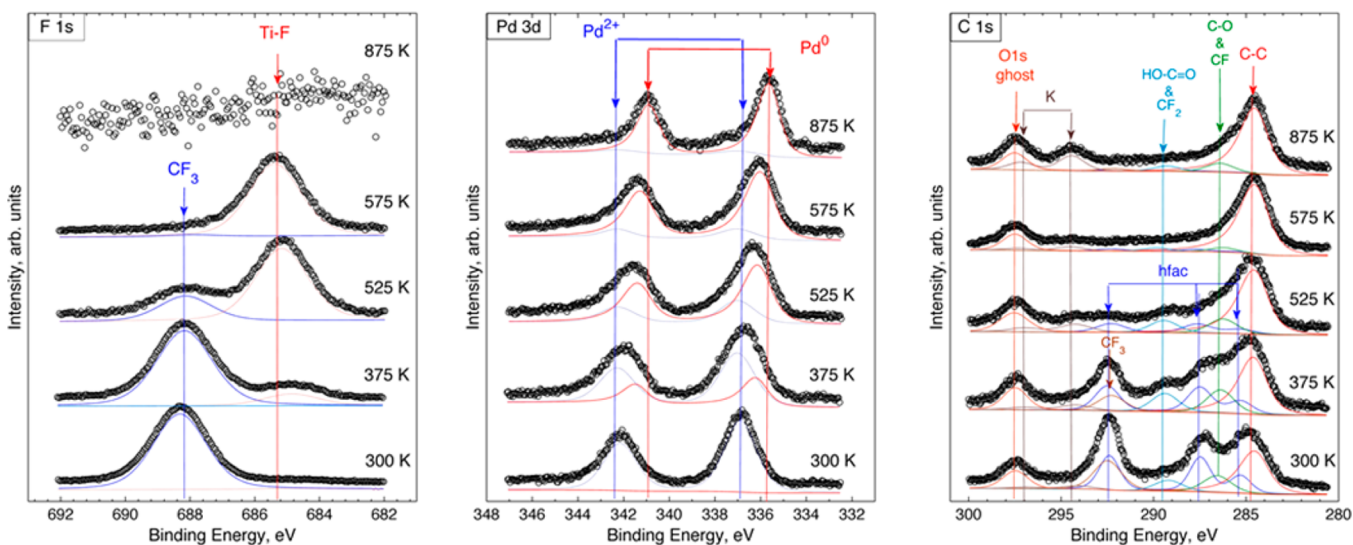
Figure 2. F 1s, Pd 3d and C 1s XPS spectra obtained following TiO$_2$(110) exposed to Pd(hfac)$_2$ at 300 K and heated at 375, 525, 575, 775, and 875 K. The spectra were collected at the specified temperature.

1 based on the Pd 3d, C 1s, and F 1s peaks, and the results are summarized in Tables 2 and 3.

The observed trend in these calculations demonstrated that (i) the hfac coverage does not change with adsorption temperature, (ii) the extent of hfac cracking increased, and (iii) the amount of palladium increases. The conclusion is that, at elevated adsorption temperatures, some products of Pd(hfac)$_2$ decomposition desorb, leaving palladium atoms on the surface. This assumption is supported by the observation of the Pd 3d$_{5/2}$ peak at 336.2 eV assigned to a PdO$_x$ species and/or Pd clusters.

Thermal decomposition of the adlayer prepared by exposure of TiO$_2$(110) to Pd(hfac)$_2$ at 300 K was studied by heating in a stepwise manner from 300 to 875 K under UHV. Relevant XPS spectra are shown in Figure 2.

Following heating at 575 K, the CF$_3$ species represented by the F 1s peak at 688.3 eV was replaced by the Ti−F species, represented by the F 1s peak at 684.9 eV. The Ti−F species decomposed completely following heating at 875 K. In the Pd 3d region, heating to 375 K resulted in the appearance of a Pd 3d$_{5/2}$ peak at 336.2 eV, which was assigned to a PdO$_x$ ($x < 2$) species and/or Pd clusters and/or atoms. The intensity of the Pd(hfac)$_{ads}$ components decreased reaching a plateau at 525 K, indicating decomposition of the Pd(hfac)$_{ads}$ species (Figures 2 and S2, Supporting Information). At 775 K, the Pd 3d$_{5/2}$ peak was at 335.8 eV. This BE is too low to be assigned to a PdO$_x$ species;[30] therefore, we assume that the PdO$_x$ species decomposed. However, this BE is too high for bulk metallic Pd, which is characterized by a Pd 3d$_{5/2}$ peak at 335.0 eV.[30] Thus, we conclude that this shift to a higher binding energy is caused by the size effect in Pd metal nanoparticles, which give shifts to a higher BE because of incomplete final state

relaxation.[37] With increasing temperature, the Pd 3d$_{5/2}$ peak at 335.8 eV shifted toward a lower BE and reached 335.6 eV following annealing at 875 K. The BE shift toward lower binding energies observed between 775 and 875 K is assigned to a sintering effect that partially removes the final state relaxation limitation.

Thermal decomposition of adsorbed hfac-containing species and the transformation of its dissociation fragments were traced by monitoring the coverages of different carbon species during annealing (Figures 2 and S3, Supporting Information). Coverages were calculated using eq 1. The Pd(hfac)$_{ads}$ species fully decomposes at 525 K, in agreement with the conclusion reached based on the evolution of the Pd 3d spectra (Figure 2). CF$_3$ fragments associated with the decomposition of the hfac ligand follow the same trend and, therefore, have thermal stability similar to Pd(hfac)$_{ads}$. The CF$_2$, carboxyl, and CF species are likely intermediates of Pd(hfac)$_{ads}$ and hfac$_{ads}$ decomposition. CF$_2$ and CF species might form through decomposition of CF$_3$ by transfer of fluorine atoms to TiO$_2$(110). Above 575 K, the carbon species related to hfac groups vanish, and only a single asymmetric peak related to graphitic carbon or other carbon species formed by decomposition of the organic moieties could be detected. The carbon remaining following annealing at 875 K is likely graphitic. Potassium, a bulk crystal contaminate, diffuses from the bulk to the surface during annealing at 875 K.

Detailed XPS analysis of surface chemical states also revealed possible adsorption sites for Pd(hfac)$_{ads}$ and hfac$_{ads}$. The clean TiO$_2$(110) surface was characterized by the Ti 2p$_{3/2}$ peak at 459.3 eV, which is a feature of stoichiometric TiO$_2$. An additional Ti 2p$_{3/2}$ peak at 457.5 eV assigned to reduced titania,

14706

dx.doi.org/10.1021/am504127k | ACS Appl. Mater. Interfaces 2014, 6, 14702−14711

TiO_x ($x < 2$), was also observed (spectra are shown in Figure S4, Supporting Information).

The evolution of the TiO_x and TiO_2 components is shown in Figure 3. The TiO_x component disappears following $Pd(hfac)_2$
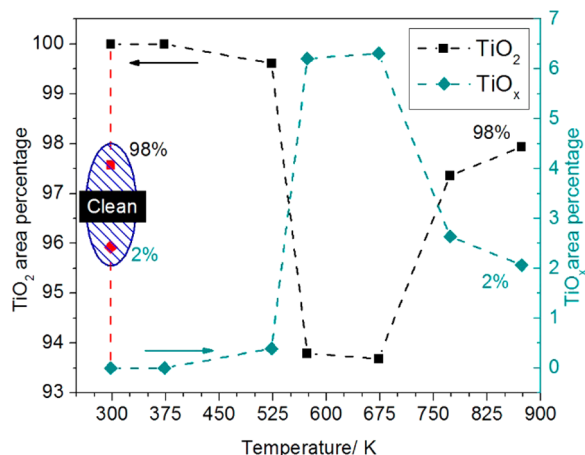

Figure 3. Changes in area percentage of TiO_2 and TiO_x components upon heating for clean $TiO_2(110)$, $Pd(hfac)_2$ exposure at 300 K, and during annealing to 875 K. The shaded area shows the fractions of TiO_2 and TiO_x for the clean $TiO_2(110)$ single crystal before the $Pd(hfac)_2$ exposure.

adsorption. However, the TiO_x peaks reappeared upon heating to 525 K, the same temperature at which the $Pd(hfac)_{ads}$ and $hfac_{ads}$ species decomposed. This suggests that the reduced titania centers are involved in $Pd(hfac)_2$ adsorption and/or dissociation. The oxygen atoms of the hfac ligand might interact with the reduced TiO_x centers providing oxygen needed for a fully oxidized surface. Following decomposition of the $hfac_{ads}$ ligands at 575 K in UHV, the TiO_x area percentage increases to ~6.5% before returning to the original value of ~2% following heating at 875 K (Figure 3). The increase of the TiO_x contribution at 575 K might be due to the reaction of the surface oxygen from stoichiometric TiO_2 with carbon fragments from the hfac ligands. Heating to 875 K results in the diffusion of the oxygen vacancies to the bulk and return of the surface to its initial state.

The number of $Pd(hfac)_2$ adsorption and decomposition cycles on the $TiO_2(110)$ surface determines the amount of the deposited Pd. Palladium coverages and palladium layer thicknesses are shown in Figure 4 for four consecutive cycles of $Pd(hfac)_2$ adsorption at 300 K followed by heating to 875 K in UHV. XPS spectra for consecutive cycles are similar to those for the first deposition cycle. In addition to the Pd coverage, the thicknesses are presented for comparison with the value of growth per cycle (GPC) for $Pd(hfac)_2$ ALD measured by quartz crystal microbalance (QCM), which assumes formation of a uniform overlayer after each cycle. Similarly, we have used a uniform Pd overlayer XPS quantification model. The details of the thickness calculations are provided in the Supporting Information. Growth is linear, with a GPC of 0.6 Å (Figure 4). Therefore, the amount of deposited palladium can be controlled by the number of adsorption and decomposition cycles. The linear growth of Pd indicates that the remaining graphite-like carbon does not block adsorption sites for $Pd(hfac)_2$.

3.2. Scanning Tunneling Microscopy. To complement the XPS results with topography data, an STM investigation
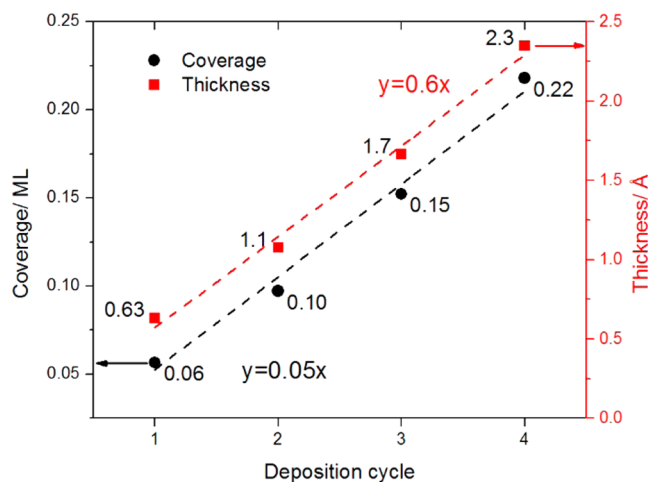

Figure 4. Pd growth curve showing the coverage of the Pd in ML versus number of deposition cycles. Each cycle consists of adsorption of $Pd(hfac)_2$ at 300 K followed by annealing in UHV to 875 K.

was performed. A typical 100×100 nm STM image of the clean $TiO_2(110)$ surface following the preparation procedure, described in the Experimental Methods section, is shown in Figure 5A. Irregularly shaped terraces are present, as are defect sites that show up as bright spots and added rows. The spots might be oxygen vacancies or other defect types, and the added rows act as precursors for the $TiO_2(110)$-(1×2) surface reconstruction.[38] The measured step height was approximately 3.2 ± 0.2 Å, in agreement with the expected value of 3.24 Å for rutile $TiO_2(110)$. Alternating bright and dark rows running along the $[001]$ direction are visible. The spacing between bright rows and between dark rows in the $[1\bar{1}0]$ direction is approximately 6.5 Å. Within bright rows, the spacing between features was approximately 3 Å. Atomic resolution data after Fourier transform filtering is shown in the inset in Figure 5A with the dimensions labeled. These dimensions correspond to a bulk terminated $TiO_2(110)$-(1×1) surface, where the bright features are attributed to surface 5-fold Ti atoms and the dark features to bridging oxygen atoms.[38]

A 100×100 nm image following saturation dosing of $Pd(hfac)_2$ at RT is shown in Figure 5B. This surface is characterized by bright clusters with similar approximate size and density as the defect sites on the clean TiO_2, and bright, discontinuous rows running along the $[001]$ direction with inter-row spacing of approximately 6.5 Å. Though the discontinuities could not be resolved in all images, a Fourier transform of an area containing discrete features revealed their spacing along a row in the $[001]$ direction to be approximately 6 Å (inset, Figure 5B). The dimensions of these dark and bright spots correspond to a structured (2×1) overlayer, which can be assigned to bidentate bridging hfac ligands bonding through both oxygen atoms to two 5-fold Ti atoms, and $Pd(hfac)_{ads}$ with Pd bonding to two surface bridging oxygen atoms shown schematically in the ball model in Figure 6. The contrast in the STM images allows to identify the adsorption species and adsorption sites: Pd(hfac), if bound between two bridging oxygen atoms, would protrude further from the surface than an hfac ligand bound to two 5-fold coordinated Ti atoms, and would therefore appear brighter on the basis of topography. Based solely on topography, then, the adsorbed hfac ligands would appear as the dark spots also in a (2×1) arrangement. The contrast may also be explained by electronic arguments.
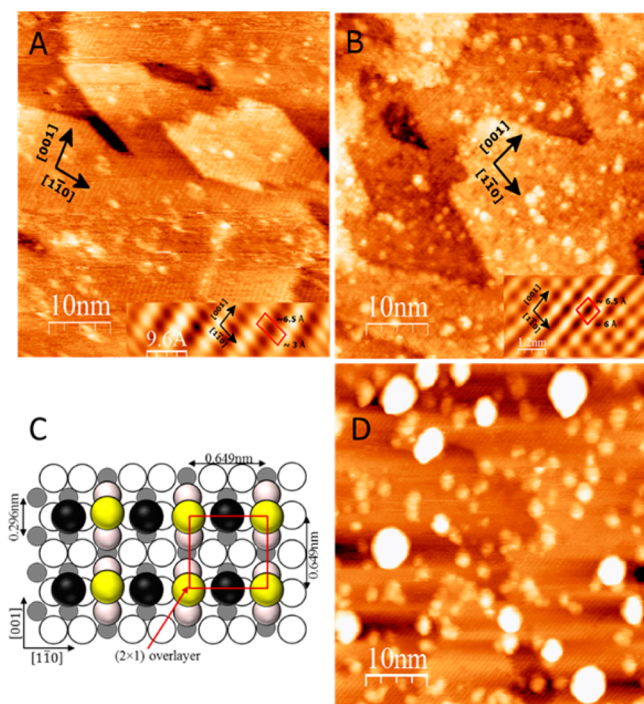
Figure 5. STM images of the $TiO_2(110)$ surface. A: Clean $TiO_2(110)$ following sputtering and annealing cycles ($V = +2.0$ V, $I = 70$ pA). Inset: atomic scale image after Fourier transform showing the unreconstructed (1×1) unit cell. B: TiO_2 following dosing of $Pd(hfac)_2$ for 60 min at room temperature ($V = +1.75$ V, $I = 0.1$ nA). Inset: small scale image after Fourier transform showing structured (2×1) overlayer of adsorbates. The bright spots are assigned to $Pd(hfac)_{ads}$ group. C: Model for $Pd(hfac)_2$ adsorbed on $TiO_2(110)$: The $Pd(hfac)_2$ dissociates. The resulting hfac (hfac: black spheres) binds to two 5-fold coordinated Ti atoms (gray spheres) in a bidentate fashion and the Pd(hfac) (Pd(hfac): yellow spheres) adsorbs between two bridging oxygen (oxygen: white spheres). The adsorption geometry matches the experimental value reported in the image B inset. D: Following annealing of the as-deposited sample to 875 K for 20 min ($V = +0.5$ V, $I = 2.0$ nA).
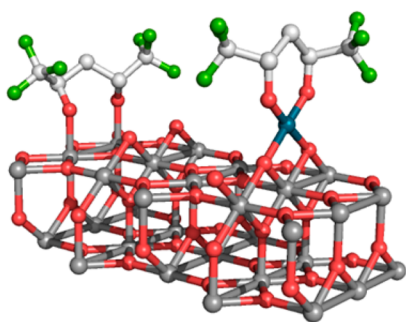
Figure 6. $Pd(hfac)_2$ molecule adsorbed on the $TiO_2(110)$ surface at room temperature. $Pd(hfac)_2$ dissociates into a $hfac_{ads}$ ligand, which bonds across neighboring 5-fold coordinated Ti sites (gray atoms), and a Pd(hfac), which bonds across bridging O atoms (red atoms) on the surface. Adsorbed Pd(hfac) is responsible for the (2×1) structure observed after $Pd(hfac)_2$ adsorption at room temperature. Adjacent Pd(hfac) and hfac groups are not shown for clarity.

For example, the appearance of dark and bright areas was reported in the STM images of the Si(111)-(7×7) surface exposed to $Cu(hfac)_2$.[39] On the basis of the bias dependence, dark areas were assigned to hfac ligands and the bright regions

to Cu atoms when empty electronic states of the sample were tested at positive bias voltage. The STM images shown in Figure 5 were obtained at positive biases. Therefore, hfac ligands might appear as the dark rows. The $Pd(hfac)_{ads}$ species is expected to have a higher density of states above the Fermi level than those for the $hfac_{ads}$ group, leading to the $Pd(hfac)_{ads}$ species appearing as the bright spots (Figure 5B). Unfortunately, the $Pd(hfac)_{ads}$ + $(hfac)_{ads}$ adlayer was not stable under the LEED electron beam, and therefore the LEED patterns were not collected.

The proposed model for dissociative $Pd(hfac)_2$ adsorption on $TiO_2(110)$ is in agreement with an observed (2×1) overlayer following dosing of $Cu(hfac)_2$ on $TiO_2(110)$.[20,40] The authors of that study noted that the distance of the two oxygen atoms in the hfac ligand of $Cu(hfac)_2$ is 2.79 Å, close to the distance of 2.96 Å between two 5-fold surface Ti atoms on $TiO_2(110)$, which makes that site suitable for adsorption of hfac. This is close to the value of 2.77 Å between two O atoms in an hfac ligand in $Pd(hfac)_2$.[41]

Following annealing at 575 K, nanoparticles appeared with an average height of 1.2 ± 0.6 nm (the STM images are shown in the Supporting Information, Figure S5), where the error is one standard deviation from the average value. Uncertainty in the height distribution arises from the difficulty in determining which features are Pd nanoparticles, which are agglomerations of ligand fragments, and which are original defects in the TiO_2 surface. The best quality images were obtained at lower bias and higher tunneling current ($V = +0.8$ V, $I = 1.0$ nA) than for the previous experiment, indicating that surface conductivity had increased. This might be due to the formation of Pd nanoparticles.

Annealing at 875 K resulted in the agglomeration of the nanoparticles, and the unreconstructed $TiO_2(110)$-(1×1) surface reappeared, as shown in Figure 5D. These results agree with the XPS data, which demonstrated the complete decomposition of the $(hfac)_{ads}$ species at 575 K and Pd nanoparticle sintering at 875 K. The average height of the nanoparticles was 1.7 ± 0.5 nm at 875 K. Even after annealing to 875 K, the particle size is within the range where a size-dependent BE shift could be observed. Therefore, the +0.6 eV shift of the Pd $3d_{5/2}$ peak from the peak position for the bulk palladium (335.0 eV) could be assigned to a particle size effect. No preferential nucleation of the Pd NPs was observed at step edges. The coverage of Pd particles was estimated from the STM data to be 0.03 ML at 875 K. This value is in good agreement with the 0.05 ML calculated using the XPS data. It must be noted that the apparent lateral dimension of these nanoparticles depends on the STM tip shape and, therefore, is not used. The coverage estimation from STM assumes a hemispherical nanoparticle shape in which the radius is approximately equal to the height.

4. DISCUSSION

On the basis of the experimental data, the mechanism shown in Figure 7 is proposed for the interaction of $Pd(hfac)_2$ with $TiO_2(110)$. The cleaning procedure of $TiO_2(110)$ causes thermal desorption of surface oxygen leaving behind a partially reduced surface with TiO_x species.[38] Upon adsorption at 300–450 K, the $Pd(hfac)_2$ precursor dissociates to $(hfac)_{ads}$ and $Pd(hfac)_{ads}$ species. Further decomposition of the $(hfac)_{ads}$ and $Pd(hfac)_{ads}$ species occurs at 375 and 450 K. The $(hfac)_{ads}$ and $Pd(hfac)_{ads}$ species form a (2×1) surface overlayer. The hfac fragment adsorbs in a bidentate bridging fashion across two Ti
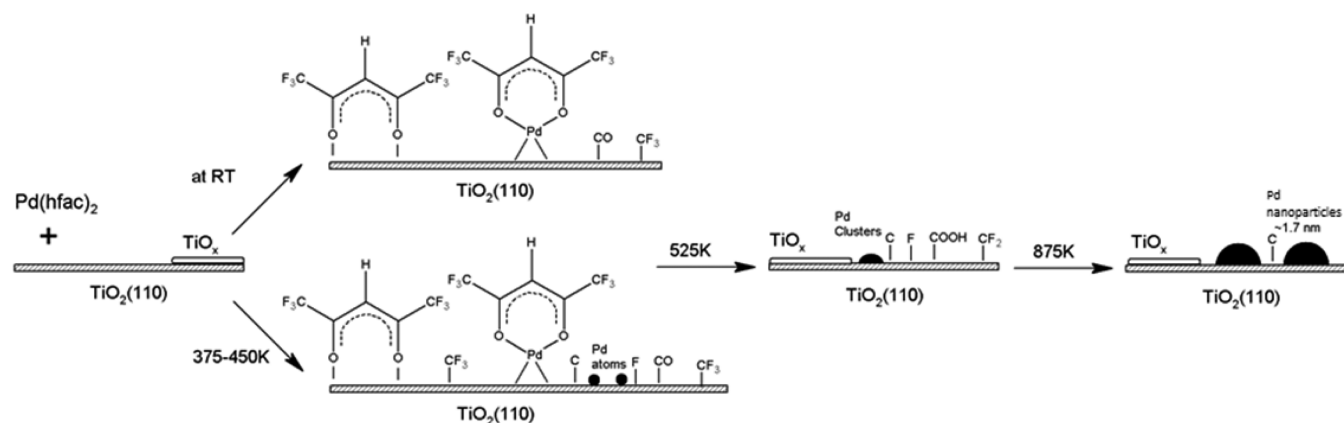
Figure 7. Schematic of the reaction of Pd(hfac)₂ with a TiO₂(110) surface.

5-fold atoms and Pd(hfac) adsorbs between two bridging oxygen atoms (Figure 6). Following Pd(hfac)₂ adsorption, the TiOₓ species disappeared, showing that hfac$_{ads}$ and its cracked fragments reoxidize the surface (Figure 3). This implies that in a parallel path with the adsorption on Ti 5-fold atoms, the hfac$_{ads}$ species can adsorb on the TiOₓ defects and compensate for the lack of oxygen.

Cracked fragments of the hfac ligand were observed at all adsorption temperatures. The degree of hfac decomposition increases with increasing adsorption temperature. Heating the adsorbed layer resulted in decomposition of the Pd(hfac)$_{ads}$ and (hfac)$_{ads}$ species, which dissociated at approximately 525 K, leaving the cracked hfac fragments and Pd^0 clusters (Figure 7). The CF₃ species underwent decomposition through sequential loss of fluorine atoms, which then bond to titanium. Ti−F species were observed on the surface up to 775 K. No fluorine-containing species were detected at 875 K. Carbon atoms segregate to graphitic-like (C−C) structures at 575 K. The rest of the carbon-containing species partially desorb: the carbon level decreases upon heating until 675 K and then remains unchanged upon further annealing to 875 K. Once the hfac groups thermally decomposed at 525 K, reduced titania appeared on the surface. At 875 K, the level of reduced titania returned to the original level of the clean TiO₂(110) surface due to diffusion of surface oxygen vacancies to the bulk (Figure 3).

Following annealing at 775 K, the Pd coverage decreased to 0.07 ML, indicating sintering of the Pd nanoparticles, which is accompanied by the Pd 3d$_{5/2}$ peak shifting toward a lower BE. This BE shift is attributed to the formation of larger Pd nanoparticles. It could also be attributed to the encapsulation of Pd nanoparticles by TiOₓ species; however, for Pd particle encapsulation to take place, the TiO₂ support must first be reduced.[42] Here, the TiOₓ component decreases continuously upon annealing to 875 K, which indicates absence of encapsulation in our system.

Because hfac$_{ads}$ and its cracked fragments can block Pd(hfac)₂ adsorption, their removal is critical for the next deposition cycles. As shown in Figure 4, on the surface free of hfac ligands and decomposition fragments, the amount of palladium linearly increases with the number of deposition cycles. The key factor for linear growth was thermal decomposition and removal of the hfac ligands at 875 K prior to each cycle of the Pd(hfac)₂ adsorption. On the other hand, for a real Pd(hfac)₂ ALD process, the number of typical ALD cycles required to reach steady-state Pd ALD growth was reported to be between 20 to 100 ALD cycles.[8] QCM measurements for Pd(hfac)₂/formalin ALD on TiO₂ showed 0.22 Å growth per cycle.[16] This is about 1/3 of the value of 0.6 Å per cycle calculated from our XPS data. The residual fluorine- and carbon-containing contaminations might cause surface poisoning during the first few cycles (see for instance Figure 3 in Elam et al.[8]). The contaminations could be a reason for the lower growth per cycle. Surface blocking by hfac$_{ads}$ and its fragment moieties was assumed to be responsible for Pd nucleation delay on the Al₂O₃ and TiO₂ surfaces.[8,15,16]

Following annealing at 875 K, Pd nanoparticles with an average height of 1.7 ± 0.5 nm were obtained. Assuming a hemispherical shape of the particle, the average diameter at the base of the particle is 3.4 ± 1.0 nm. The Pd coverage was estimated to be 0.1 ML after Pd(hfac)₂ exposure, and 0.03−0.05 ML after annealing at 875 K, respectively.

5. CONCLUSIONS

Pd(hfac)₂ adsorption is a self-limiting reaction on the TiO₂(110) surface yielding Pd(hfac)$_{ads}$ and/or hfac$_{ads}$ species and partial hfac fragmentation at room temperature. The removal of the hfac ligand and its fragments through thermal decomposition eliminates the initial growth delay period and results in linear growth of Pd on the TiO₂(110) surface. The Pd amount linearly increases with the number of adsorption/dissociation cycles with an average growth per deposition cycle of about 0.05 ML (0.6 Å).

■ ASSOCIATED CONTENT

ⓈSupporting Information

Derivation of coverage and thickness XPS models and required parameters are provided along with additional XPS spectra, coverage of carbon species observed during heating experiments and STM figures for the intermediate annealing temperature. This material is available free of charge via the Internet at http://pubs.acs.org.

■ AUTHOR INFORMATION

Corresponding Author

*Dr. Dmitry Zemlyanov. Address: Birck Nanotechnology Center, Purdue University, 1205 W. State Street, West Lafayette, IN 47906, United States. E-mail: dzemlian@purdue.edu.

■ REFERENCES

(1) Biffis, A.; Zecca, M.; Basato, M. Palladium Metal Catalysts in Heck C-C Coupling Reactions. *J. Mol. Catal. A: Chem.* **2001**, *173*, 249−274.

(2) Molnár, Á.; Sárkány, A.; Varga, M. Hydrogenation of Carbon−Carbon Multiple Bonds: Chemo-, Regio- and Stereo-Selectivity. *J. Mol. Catal. A: Chem.* **2001**, *173*, 185−221.

(3) Blaser, H.-U.; Indolese, A.; Schnyder, A.; Steiner, H.; Studer, M. Supported Palladium Catalysts for Fine Chemicals Synthesis. *J. Mol. Catal. A: Chem.* **2001**, *173*, 3−18.

(4) Zhu, G.; Han, J.; Zemlyanov, D. Y.; Ribeiro, F. H. Temperature Dependence of the Kinetics for the Complete Oxidation of Methane on Palladium and Palladium Oxide. *J. Phys. Chem. B* **2004**, *109*, 2331−2337.

(5) Gabasch, H.; Kleimenov, E.; Teschner, D.; Zafeiratos, S.; Hävecker, M.; Knop-Gericke, A.; Schlögl, R.; Zemlyanov, D.; Aszalos-Kiss, B.; Hayek, K.; Klötzer, B. Carbon Incorporation During Ethene Oxidation on Pd(111) Studied by in Situ X-Ray Photoelectron Spectroscopy at 2×10^{-3} mbar. *J. Catal.* **2006**, *242*, 340−348.

(6) Newton, M. A.; Belver-Coldeira, C.; Martinez-Arias, A.; Fernandez-Garcia, M. Dynamic in Situ Observation of Rapid Size and Shape Change of Supported Pd Nanoparticles During CO/NO Cycling. *Nat. Mater.* **2007**, *6*, 528−532.

(7) Feng, H.; Lu, J.; Stair, P.; Elam, J. Alumina Over-Coating on Pd Nanoparticle Catalysts by Atomic Layer Deposition: Enhanced Stability and Reactivity. *Catal. Lett.* **2011**, *141*, 512−517.

(8) Elam, J. W.; Zinovev, A.; Han, C. Y.; Wang, H. H.; Welp, U.; Hryn, J. N.; Pellin, M. J. Atomic Layer Deposition of Palladium Films on Al_2O_3 Surfaces. *Thin Solid Films* **2006**, *515*, 1664−1673.

(9) Lu, J.; Fu, B.; Kung, M. C.; Xiao, G.; Elam, J. W.; Kung, H. H.; Stair, P. C. Coking- and Sintering-Resistant Palladium Catalysts Achieved through Atomic Layer Deposition. *Science* **2012**, *335*, 1205−1208.

(10) Feng, H.; Elam, J. W.; Libera, J. A.; Setthapun, W.; Stair, P. C. Palladium Catalysts Synthesized by Atomic Layer Deposition for Methanol Decomposition. *Chem. Mater.* **2010**, *22*, 3133−3142.

(11) Lu, J.; Liu, B.; Greeley, J. P.; Feng, Z.; Libera, J. A.; Lei, Y.; Bedzyk, M. J.; Stair, P. C.; Elam, J. W. Porous Alumina Protective Coatings on Palladium Nanoparticles by Self-Poisoned Atomic Layer Deposition. *Chem. Mater.* **2012**, *24*, 2047−2055.

(12) Feng, H.; Libera, J. A.; Stair, P. C.; Miller, J. T.; Elam, J. W. Subnanometer Palladium Particles Synthesized by Atomic Layer Deposition. *ACS Catal.* **2011**, *1*, 665−673.

(13) Rikkinen, E.; Santasalo-Aarnio, A.; Airaksinen, S.; Borghei, M.; Viitanen, V.; Sainio, J.; Kauppinen, E. I.; Kallio, T.; Krause, A. O. I. Atomic Layer Deposition Preparation of Pd Nanoparticles on a Porous Carbon Support for Alcohol Oxidation. *J. Phys. Chem. C* **2011**, *115*, 23067−23073.

(14) Hämäläinen, J.; Ritala, M.; Leskelä, M. Atomic Layer Deposition of Noble Metals and Their Oxides. *Chem. Mater.* **2013**, *26*, 786−801.

(15) Goldstein, D. N.; George, S. M. Surface Poisoning in the Nucleation and Growth of Palladium Atomic Layer Deposition with Pd(hfac)$_2$ and Formalin. *Thin Solid Films* **2011**, *519*, 5339−5347.

(16) Lu, J.; Stair, P. C. Nano/Subnanometer Pd Nanoparticles on Oxide Supports Synthesized by AB-Type and Low-Temperature ABC-Type Atomic Layer Deposition: Growth and Morphology. *Langmuir* **2010**, *26*, 16486−16495.

(17) Weber, M. J.; Mackus, A. J. M.; Verheijen, M. A.; Longo, V.; Bol, A. A.; Kessels, W. M. M. Atomic Layer Deposition of High-Purity Palladium Films from Pd(hfac)$_2$ and H_2 and O_2 Plasmas. *J. Phys. Chem. C* **2014**, *118*, 8702−8711.

(18) Anderson, V. R.; Leick, N.; Clancey, J. W.; Hurst, K. E.; Jones, K. M.; Dillon, A. C.; George, S. M. Atomic Layer Deposition of Platinum Nanoparticles on Titanium Oxide and Tungsten Oxide Using Platinum(II) Hexafluoroacetylacetonate and Formalin as the Reactants. *J. Phys. Chem. C* **2014**, *118*, 8960−8970.

(19) Parmeter, J. E. Copper CVD Chemistry on a Reactive Substrate: Cu(hfac)$_2$ and hfacH on Pt(111). *J. Phys. Chem.* **1993**, *97*, 11530−11541.

(20) Mulley, J. S.; Bennett, R. A.; Dhanak, V. R. Adsorption, Orientation and Thermal Decomposition of Copper(II) Hexafluoroacetylacetonate on Rutile TiO$_2$(110). *Surf. Sci.* **2008**, *602*, 2967−2974.

(21) Lei, Y.; Lu, J.; Zhao, H.; Liu, B.; Low, K.-B.; Wu, T.; Libera, J. A.; Greeley, J. P.; Chupas, P. J.; Miller, J. T.; Elam, J. W. Resolving Precursor Deligation, Surface Species Evolution, and Nanoparticle Nucleation During Palladium Atomic Layer Deposition. *J. Phys. Chem. C* **2013**, *117*, 11141−11148.

(22) Zaera, F. The Surface Chemistry of Atomic Layer Depositions of Solid Thin Films. *J. Phys. Chem. Lett.* **2012**, *3*, 1301−1309.

(23) Horcas, I.; Fernandez, R.; Gomez-Rodriguez, J. M.; Colchero, J.; Gomez-Herrero, J.; Baro, A. M. WSXM: A Software for Scanning Probe Microscopy and a Tool for Nanotechnology. *Rev. Sci. Instrum.* **2007**, *78*, 013705-1−013705-8.

(24) Diebold, U.; Li, M.; Dulub, O.; Hebenstreit, E. L. D.; Hebenstreit, W. The Relationship between Bulk and Surface Properties of Rutile TiO$_2$(110). *Surf. Rev. Lett.* **2000**, *7*, 613−617.

(25) Fadley, C. S. Basic Concepts of X-Ray Photoelectron Spectroscopy. In *Electron Spectroscopy: Theory, Techniques and Applications*; Brundel, C. R., Baker, A. D., Eds.; Academic Press: New York, 1978; Vol. 2, pp 1−156.

(26) Scofield, J. H. Hartree-Slater Subshell Photoionization Cross-Sections at 1254 and 1487 eV. *J. Electron Spectrosc. Relat. Phenom.* **1976**, *8*, 129−137.

(27) Yeh, J. J.; Lindau, I. Atomic Subshell Photoionization Cross Sections and Asymmetry Parameters: $1 \leqslant Z \leqslant 103$. *At. Data Nucl. Data Tables* **1985**, *32*, 1−155.

(28) Powell, C. J.; Jablonski, A. *NIST Electron Effective-Attenuation-Length Database - Version 1.3*; National Institute of Standards and Technology: Gaithersburg, MD, 2011.

(29) Yu, J. C.; Yu; Ho; Jiang; Zhang. Effects of F⁻ Doping on the Photocatalytic Activity and Microstructures of Nanocrystalline TiO$_2$ Powders. *Chem. Mater.* **2002**, *14*, 3808−3816.

(30) Gabasch, H.; Unterberger, W.; Hayek, K.; Kloetzer, B.; Kleimenov, E.; Teschner, D.; Zafeiratos, S.; Haevecker, M.; Knop-Gericke, A.; Schloegl, R.; Han, J.; Ribeiro, F. H.; Aszalos-Kiss, B.; Curtin, T.; Zemlyanov, D. In Situ XPS Study of Pd(111) Oxidation at Elevated Pressure, Part 2: Palladium Oxidation in the 10^{-1} mbar Range. *Surf. Sci.* **2006**, *600*, 2980−2989.

(31) Lin, W. B.; Wiegand, B. C.; Nuzzo, R. G.; Girolami, G. S. Mechanistic Studies of Palladium Thin Film Growth from Palladium-(II) Beta-Diketonates. 1. Spectroscopic Studies of the Reactions of Bis(hexafluoroacetylacetonato)palladium(II) on Copper Surfaces. *J. Am. Chem. Soc.* **1996**, *118*, 5977−5987.

(32) Beamson, G.; Briggs, D. *High Resolution XPS of Organic Polymers: The Scienta ESCA300 Database*; Wiley: New York, 1992.

(33) Cohen, S. L.; Liehr, M.; Kasi, S. Mechanisms of Copper Chemical Vapor Deposition. *Appl. Phys. Lett.* **1992**, *60*, 50−52.

(34) Cohen, S. L.; Liehr, M.; Kasi, S. Selectivity in Copper Chemical Vapor Deposition. *Appl. Phys. Lett.* **1992**, *60*, 1585−1587.

(35) Donnelly, V. M.; Gross, M. E. Copper Metalorganic Chemical Vapor Deposition Reactions of Hexafluoroacetylacetonate Cu(I) Vinyltrimethylsilane and Bis (Hexafluoroacetylacetonate) Cu(II) Adsorbed on Titanium Nitride. *J. Vac. Sci. Technol., A* **1993**, *11*, 66−77.

(36) Lin, W. B.; Nuzzo, R. G.; Girolami, G. S. Mechanistic Studies of Palladium Thin Film Growth from Palladium(II) Beta-Diketonates. 2. Kinetic Analysis of the Transmetalation Reaction of Bis-(hexafluoroacetylacetonato)palladium(II) on Copper Surfaces. *J. Am. Chem. Soc.* **1996**, *118*, 5988−5996.

(37) Cheung, T. T. P. Lineshape Studies of the X-Ray Photoemission of Small Metal Clusters. *Surf. Sci.* **1983**, *127*, L129−L134.

(38) Diebold, U. The Surface Science of Titanium Dioxide. *Surf. Sci. Rep.* **2003**, *48*, 53−229.

(39) Horton, J. H.; Shapter, J. G.; Cheng, T.; Lennard, W. N.; Norton, P. R. STM Investigation of a Cu Organometallic Complex Adsorbed on Si(111)-(7 × 7). *Surf. Sci.* **1997**, *375*, 171−182.

(40) Rayner, D. G.; Mulley, J. S.; Bennett, R. A. Copper Deposition on TiO_2 from Copper(II) Hexafluoroacetylacetonate. *J. Vac. Sci. Technol., A* **2012**, *31*, 01A121 1−01A121 5.

(41) Siedle, A. R.; Newmark, R. A.; Pignolet, L. H. Structure of Palladium Bis(hexafluoroacetylacetonate) and the Systematics of Its Acid-Base Chemistry. *Inorg. Chem.* **1983**, *22*, 2281−2286.

(42) Bennett, R. A.; Stone, P.; Bowker, M. Pd Nanoparticle Enhanced Re-Oxidation of Non-Stoichiometric TiO_2: STM Imaging of Spillover and a New Form of SMSI. *Catal. Lett.* **1999**, *59*, 99−105.

14711

dx.doi.org/10.1021/am504127k | *ACS Appl. Mater. Interfaces* 2014, 6, 14702−14711